Estimating the Effect of Higher Order Modes in Spherical Near-Field Probe Correction

Allen Newell, Stuart Gregson

Nearfield Systems Inc.
19730 Magellan Drive,
Torrance, CA 90502-1104

ABSTRACT

This paper extends a previous simulation study (1, 2) of the effect of higher order probe modes when the spherical numerical software uses the orthogonality approach to solve for the spherical modes of the antenna under test (AUT). In this commonly used approach, the probe is assumed to have only modes for $\mu = \pm 1$, and if the probe has higher order modes, errors will be present in the calculated AUT spherical coefficients and the resulting far-field parameters. In the previous studies, a computer simulation was developed to calculate the output response for an arbitrary AUT/probe combination when the probe is placed at arbitrary locations on the measurement sphere. The planar transmission equation was used to calculate the probe response using the plane wave spectra for actual AUTs and probes derived from either planar or spherical near-field measurements. The positions and orientations of the AUT and probe were specified by a combination of rotations of the antenna's spectra and the x, y, z position of the probe used in the transmission equation. The simulation was carried out for rectangular Open Ended Waveguide (OEWG) probes using all of the higher order modes and also for the same probe where only the $\mu = \pm 1$ modes were used to calculate the probe patterns. The parameter that was used to estimate the error in the measured near-field data was the RMS combination of the complex differences between near-field polarization curves over a χ rotation span of 100º. This RMS combination represented the estimated error signal level relative to the peak near-field amplitude. Using two different AUTs, different measurement radii and a sequence of θ-positions on the measurement sphere, the error signal levels were between -35 and -80 dB and the initial conclusion was that the effect of the higher order modes on typical measurements using OEWG probes would be smaller than other typical measurement errors and therefore have little practical effect on far-field results.

In this phase of the study the goal was to develop general guidelines to predict the error signal level for a given AUT/probe/measurement radius combination. The same simulation software was used in this study with the following changes and additions. Rather than use all of the points in the polarization curves to derive an RMS error signal level, only the χ-rotation angles of 0º and 90º were used since these are the only two probe rotation angles used in a typical spherical near-field measurement. In addition to deriving the error estimates for specific spherical angles and measurement radii, complete sets of near-field data were derived for some cases, the far-fields calculated and compared to derive estimates of far-field error levels.

The results of these simulations are presented and guidelines developed to aid in the choice of spherical near-field probes and measurement radii for typical antennas.

1.0 Introduction

The spherical near-field theory is based on the transmission equation derived by Jensen (3) – (4) and further developed by Wacker (5) where the antenna under test and the probe are described by spherical mode coefficients of basis functions that are solutions of Maxwell's equations for a spherical coordinate system. In principle, the spherical transmission equation is valid for any arbitrary test antenna and probe combination at any separation distance between the spherical coordinate system origin and the probe which is outside of the minimum sphere that will completely enclose the antenna under test. The transmission equation is,

$$W^a\left(\chi,\phi,\theta\right) = \sum_m \sum_n \sum_\mu \left(\sum_{s=1}^{2} P^{s\mu na} Q^{smn} \right) e^{im\phi}\, d_{m\mu}^{(n)}(\theta)\, e^{i\mu\chi}. \quad (1)$$

Where W^a is the amplitude and phase data measured by the probe at the radius a and the position defined by the spherical coordinates θ *and* ϕ. χ is the rotation angle of the probe about its z-axis. The P's are the spherical mode coefficients for the probe and the Q's are the corresponding spherical mode coefficients for the antenna under test (AUT). Mathematical orthogonality is used to solve the transmission equation in order to obtain the coupling product within the brackets of (1). The result is shown in (2).

$$I^{m'\mu'n'a} = \frac{1}{8\pi^2}\int_0^{2\pi}\int_0^{2\pi}\int_0^{2\pi} W^a(\chi,\theta,\phi)\left(e^{-im'\phi}\, d_{m'\mu}^{(n')}(\theta)\, e^{i\mu'\chi}\right)$$
$$\times \sin\theta\, d\theta\, d\phi\, d\chi, \quad (2)$$

Where,

$$I^{m'\mu'n'a} = P^{1\mu'n'a} Q^{1m'n'} + P^{2\mu'n'a} Q^{2m'n'}.$$

(3)

In order to perform the integration for the three angular variables θ, φ *and* χ using incrementally measured data, the data point spacing for all three angles must satisfy the sampling criteria for each variable. —Theoretical guidelines are available (6) to specify the angular spacing in θ and φ in terms of the radius of the minimum sphere that will completely enclose the antenna. Experimental tests on a given test antenna and probe can also be carried out to verify these guidelines by taking closely spaced data and comparing the far field pattern results when the data point spacing is increased. For an arbitrary probe and measurement radius, satisfying the sampling criteria for the χ variable could require measurements at small increments in χ and numerical integration of the data in χ. The required multiple measurements over the complete sphere for small increments in χ would be very time-consuming and the numerical integration could be both time-consuming and inaccurate. To solve this problem, Wacker (5) proposed using a special probe that would have a symmetry in its far field pattern such that the spherical mode coefficients for the probe would be zero for all μ values except μ = ±1. Such probes are referred to as first-order probes. When the probe satisfies this condition, measurements are only required for χ = 0º and 90º and numerical integration of the data for the χ variable is not required. This greatly reduces the measurement time and results in a fast, efficient and accurate numerical technique to perform the calculations defined in (2). The vast majority of the software used in processing spherical near-field data uses this numerical technique and the assumption that the probe satisfies the μ = ±1 requirement is implicit in using this software. Probes can be constructed which satisfy this requirement to a very high degree by using a circularly symmetric probe aperture and a precise transition from rectangular to circular waveguide. The spherical mode coefficients for μ ≠ ±1 of carefully constructed probes are typically at least 40 dB below the first order modes. But such special probes increase the cost of the measurement system and the probes may have a smaller bandwidth than similar rectangular open ended waveguide probes (OEWG). It has been established that if the measurement radius is large enough, probes such as the OEWG can be used for spherical near-field measurements and the effect of their higher order modes will be negligible and the efficient data processing algorithms can be used without causing a significant error in the results. There is only limited information (7 – 11) on how large the radius must be and what the residual effects of the higher-order modes are. This study was undertaken to try and answer some of those questions using a computer simulation technique that should be a very sensitive test of the effect of higher order probes.

2.0 Simulation Concept

The simulation has been described in detail in previous papers (1, 2) and will be summarized here.

Previously measured spherical near-field data for both the antenna under test (AUT) and a rectangular open ended waveguide (OEWG) probe is used to calculate the far-field patterns of both antennas over a full sphere. The AUT far-field pattern is then rotated mathematically about the Z-axis to simulate a φ-rotation and about the Y-axis to simulate a θ-rotation. The transmitting plane wave spectrum over the forward hemisphere on a k-space, (k_x, k_y) grid is then derived from the rotated pattern. This plane-wave spectrum represents the AUT rotated in φ and θ as it is in a spherical near-field measurement.

The far-field probe pattern is rotated about its Z-axis to simulate a χ-rotation and its receiving plane wave spectrum calculated on the same k-space grid as the AUT. The calculation of a receiving plane-wave spectrum for the rotated OEWG probe is repeated but in this case, the spherical modes for μ ≠ ±1 are set to zero in the calculation of its far-field pattern. The two spectra represent respectively a higher order probe and a first order probe with otherwise identical patterns and polarization. Figures 1 and 2 show the spherical mode amplitude plots for s=1 for the two probes.
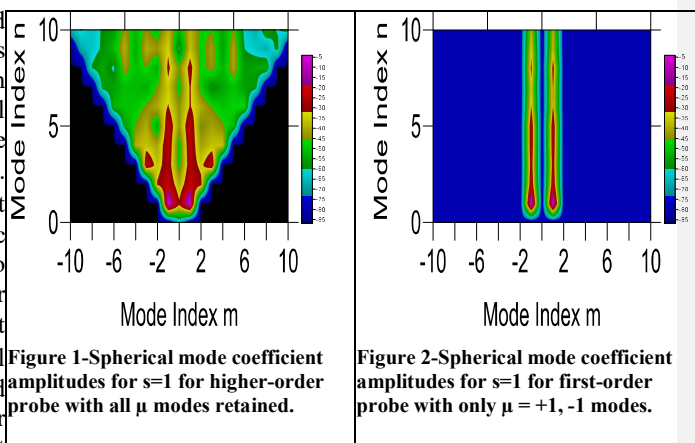

Figure 1-Spherical mode coefficient amplitudes for s=1 for higher-order probe with all μ modes retained.

Figure 2-Spherical mode coefficient amplitudes for s=1 for first-order probe with only μ = +1, -1 modes.

For the remaining steps in the simulation a computer program was developed to use the rotated plane-wave spectra of the AUT and one of the probes to calculate the output of the probe for a specified x, y, z position of the probe. When x = y = 0, the probe is at the pole of the measurement sphere and the AUT is positioned at the origin of the sphere or along the Z-axis. Offset positions of the AUT can be simulated by selecting non-zero values for x and y or using a Z-offset when calculating the AUT

far-field pattern. The z-position of the probe defines the measurement radius. The probe output is produced using the planar near-field transmission equation (7)

$$b_0'(x,y,z,\theta,\phi,\chi) =$$
$$F' a_0 \iint \vec{t}_{10}(\vec{K},\theta,\phi) \bullet \vec{s}_{02}'(\vec{K},\chi) e^{i\gamma z} e^{i(k_x x + k_y y)} dk_x dk_y$$

a_0 = Input amplitude and phase to AUT

$b_0'(x,y,z,\theta,\phi,\chi)$ = Probe output amplitude and phase for probe at (x,y,z) and rotated about the probe z-axis by the angle χ and AUT rotated by θ and ϕ

$\vec{t}_{10}(\vec{K},\theta,\phi)$ = AUT plane-wave transmitting spectrum rotated by θ and ϕ

$\vec{s}_{02}'(\vec{K},\chi)$ = Probe plane-wave receiving spectrum for χ rotation

(4)

The rotation angles $\theta, \phi, and \chi$ have been added as variables to the probe output, the AUT spectrum and the probe receiving spectrum to show that the planar transmission equation will be used to produce simulated spherical near-field data at arbitrary $\theta and \phi$ positions on the measurement sphere with arbitrary χ rotations of the probe. The planar transmission equation is used for the simulation rather than the spherical transmission equation since both are equally valid and accurate expressions for the transmission between a test antenna and a probe at any arbitrary near-field position and relative orientation. The planar equation is much easier to calculate numerically and can be used *without* modification for both first-order and higher-order probes.

The goal of the simulation is to derive general guidelines for the effect of higher order probes in spherical near-field measurements by comparing some near-field or far-field parameter obtained with the first order and higher order probes. It is not practical to simulate all the possible combinations of AUT, probe, measurement radius, AUT offset, frequency, AUT and probe rotations and density of points used in the numerical calculations. The combinations must be reduced to a manageable size and the focus should be on the parameters that are likely to have an effect on far-field results. Since the OEWG probe is widely used, it was chosen as the probe for this initial study and all the simulations are for this probe. Other probes with potentially larger amplitudes for their higher order modes can be studied in the future. Two antennas were selected for simulation. One is a narrow beam slotted waveguide array with a gain of 35 dB. The other is a pyramidal standard gain horn (SGH) with a gain of 21 dB. It is not likely that the higher order mode effect is highly sensitive to the AUT type, and these two antennas represent typical types and different gains. The frequency is 9.375 GHz, the AUT operating frequency,

and both AUTs and the probes are linearly polarized with on-axis axial ratios of 40 dB or more. It is known that the effect of the higher order modes is reduced as the measurement radius is increased and it is highly desirable to perform simulations for a large enough range of radii to derive a guideline for this parameter. It is also desirable to determine the effect on the far-field results when the higher order probe is used -and to do this; a hemisphere of near-field data must be simulated and then transformed to the far-field. A hemisphere of near-field data for the slotted array has over 50,000 data points for each of the two χ angles and this requires evaluating (4) on the order of 100,000 times. This cannot be done for many measurement radii, and so a two part approach was used.

In the first approach, complete hemisphere near-field data sets for the first order and higher order OEWG probes were generated for the slotted array at measurement radii of one and four times the minimum radius sphere, also referred to as the maximum radial extent (MRE). These were then transformed to the far-field and both the near-field data and the far-field results for the two probes compared. In the second approach, a few $\theta and \phi$ combinations were selected that would represent different amplitude, phase and polarization properties on the measurement sphere. —At these locations, the probe output was calculated using (4) for χ = 0º and 90º as a function of the radius of the measurement sphere. These curves for the first order and high order probe were then compared and error signal levels as a function of radius derived.

3.0 Complete Near-Field Simulation

Figures 3 and 4 show contour plots of the simulated θ-component (χ=0) and φ-component (χ=90) amplitudes for a measurement radius of one MRE.
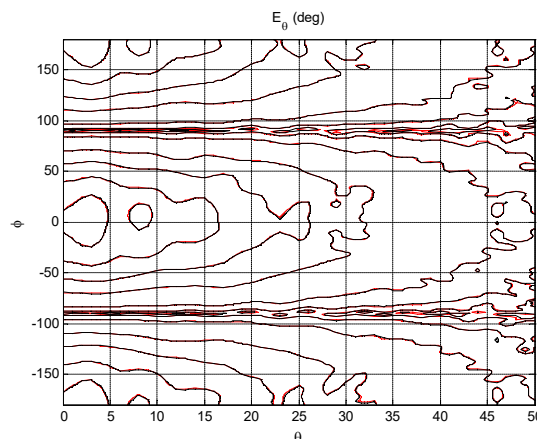

Figure 3 Simulated spherical near-field amplitude for radius = 1 MRE, (χ=0). Contour levels are -1, -3, -6, -10, -20, -30, -40, -50. Red = higher order probe, Black = first order probe.
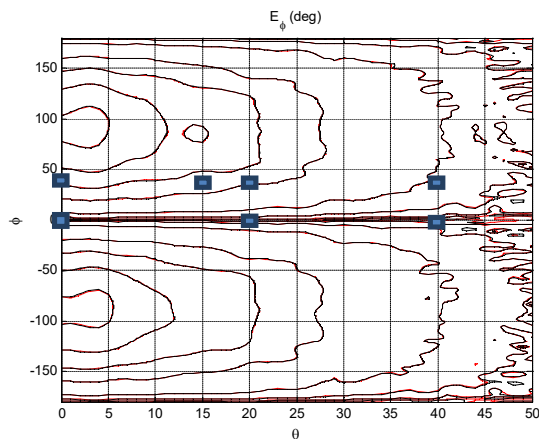
Figure 4 Simulated spherical near-field amplitude for radius = 1 MRE, (χ=90). Red = higher order probe, Black = first order probe. Small rectangles show the (θ,φ) coordinates used for the second part of the simulation to be discussed in Section 4.

Using the simulated amplitude and phase data, the amplitude of the complex difference between the near-fields for the two probes was calculated at each point and plotted relative to the peak near-field amplitude as shown in Figure 5. Using the complex difference, rather than just the amplitude difference, includes the higher order mode's effect on both the near-field amplitude and phase and represents the upper bound effect.
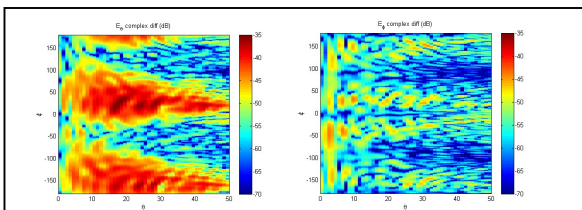
Figure 5 Amplitude of the complex difference relative to the peak near-field amplitude for (χ=0) and (χ=90) at measurement radius = 1 MRE.

There are some regions where the difference level is as high as -35 dB and other regions where it is as low as -60 to -70 dB. With this type of variation, the effect on the far-field should be less than the peak and this is confirmed when the far-field patterns are computed for the two probes and the amplitude difference converted to an error signal level. The complex difference is not used in the far-field since the far-field phase is generally not important for most antenna measurements. Figure 6 shows the far-field amplitude pattern and the error signal level difference between the two probes for the 1 MRE radius.

The peak error of -41dB occurs in the region of the main beam and the error level in the sidelobe region is below --

-60 dB. This character of the effects of probe correction errors showing up in the main beam region is consistent with other error analysis studies. If the probe pattern used for spherical processing is changed or the probe correction is neglected, it is the main beam region of the far-field that is affected.
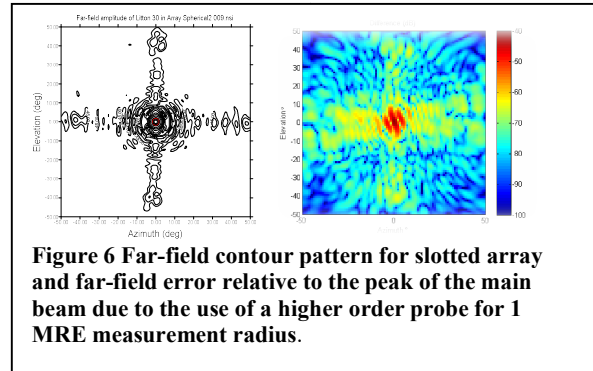

Figure 6 Far-field contour pattern for slotted array and far-field error relative to the peak of the main beam due to the use of a higher order probe for 1 MRE measurement radius.

The simulation of a complete near-field and processing to the far-field was also carried out for a measurement radius of 4 MRE and the results are shown in Figures 7 and 8. The maximum far-field amplitude difference for this case was -53 dB.
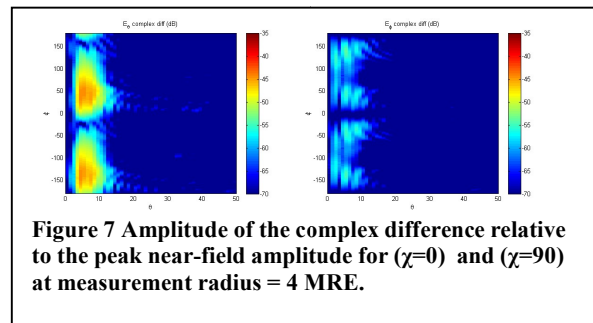

Figure 7 Amplitude of the complex difference relative to the peak near-field amplitude for (χ=0) and (χ=90) at measurement radius = 4 MRE.
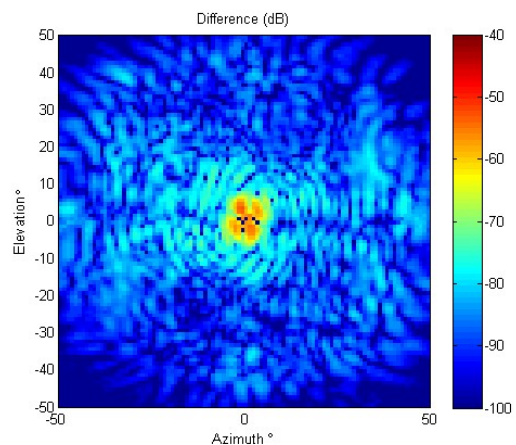

Figure 8 Far-field error relative to the peak of the main beam due to the use of a higher order probe for 4 MRE measurement radius. Peak difference = -53 dB

4.0 Simulations at Representative (θ,φ) Positions Versus Radius
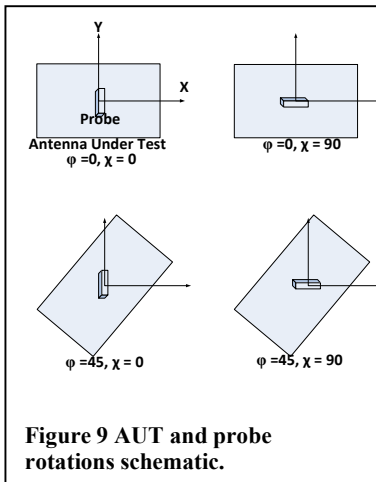

Figure 9 AUT and probe rotations schematic.

In the second approach used in the simulation, a few (θ,φ) points on the measurement sphere were selected to represent different amplitude levels, field polarizations and field complexity. Some of these points are represented by the rectangles on the contour pattern in Figure 4 and additional points at θ = 60º were also used. Most of the simulation used the φ angles of 0º and 45º, χ angles of 0º and 90º with the θ angles of 0º, 20º, 40º and 60º. Figure 9 shows a schematic representation of the rotations of the AUT in φ and the probe in χ that were applied to the patterns to produce simulated spherical data. The AUT was also rotated about its Y-axis to simulate the θ position on the sphere. The Z-value used in (4) specifies the radius of the measurement sphere.
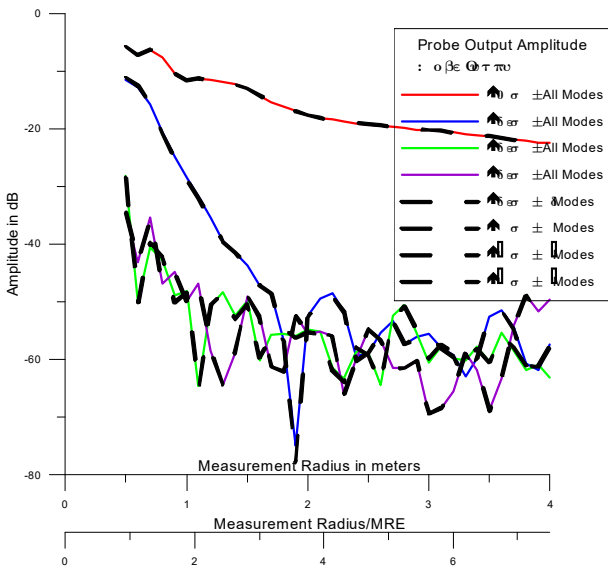

Figure 10 Simulated probe output for a first order and higher order probe at selected spherical coordinates.

Figure 10 shows plots of the simulated probe outputs as a function of Z for the case where φ=45º and χ =90º and illustrates the large variations in amplitude level, dynamic range and fine structure of the simulated spherical data.
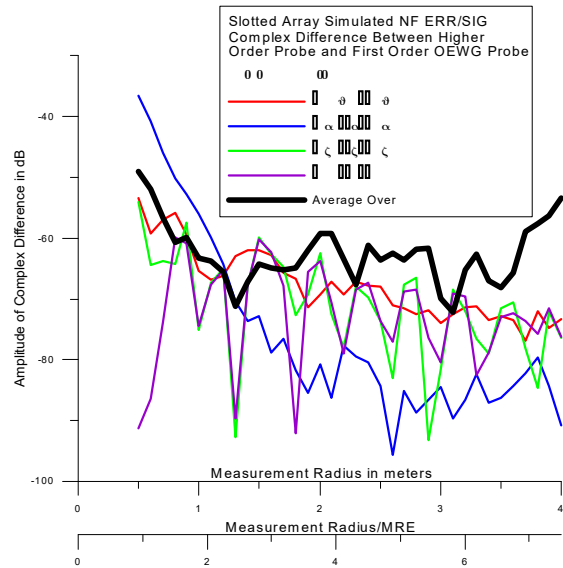

Figure 11 Amplitude of the complex difference between near-field measured with a first order and higher order OEWG probe.

The small differences between the first order and higher order probes cannot be resolved in these plots and the phase is not included, and so the complex difference is calculated at each point as shown in Figure 11.
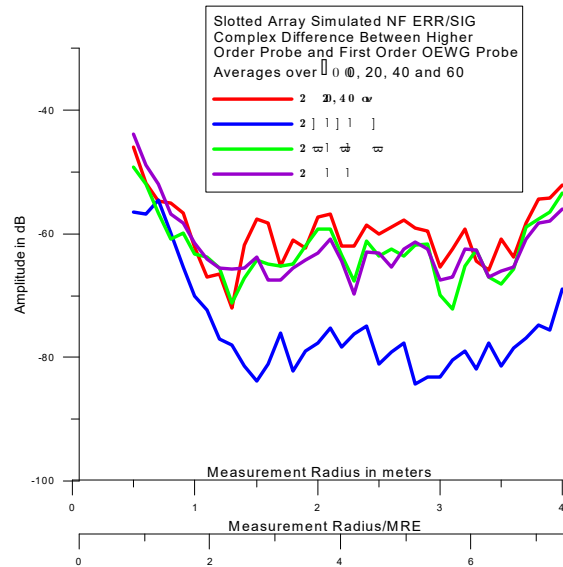

Figure 12 Averages of the complex differences for selected points on the measurement sphere for the array antenna.

The detailed shapes of the difference curves are not important in using them to predict the effect of the higher order probe and so the curves are averaged over the θ angles to produce a smother curve that is more useful. The average curve has been added to Figure 10 to illustrate the process in going from specific points on the measurement sphere to an estimate of the average effect

over the full sphere. The same averaging process was used for the other three (φ,χ) combinations illustrated in Figure 8 to produce a graphical summary of the simulation results for the second approach shown in Figure 12.

The same analysis described above was applied using the Standard Gain Horn (SGH) as the AUT and the average curves are shown in Figure 13.
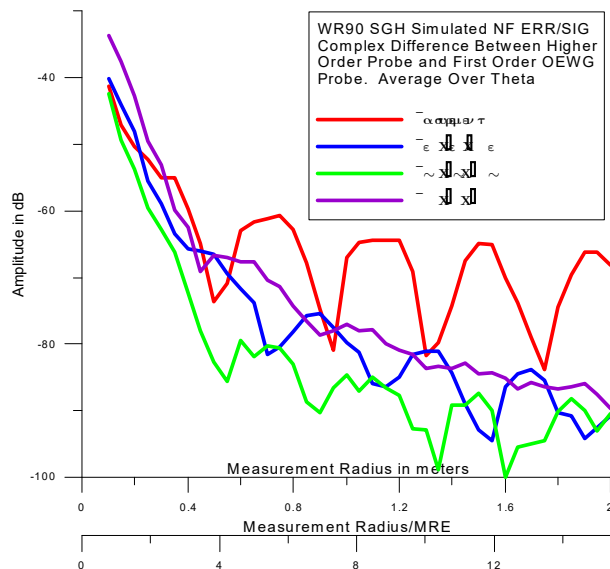

Figure 13 Averages of the complex differences for selected points on the measurement sphere for the SGH antenna.

5.0 Conclusions

-The use of the planar transmission equation to simulate near-field data on a spherical surface, and potentially other surfaces, has been demonstrated and shown to be a powerful tool for analyzing near-field measurements. Independent algorithms using different software were developed by the two authors and the very close agreement in the results substantiates the method and the implementations.

The effect of the higher order mode OEWG probe compared to an ideal first order probe decreases with distance as expected.   This is also an indication of reliability of simulations.   The results show that for radii of 2*MRE, the differences in the near-field and far-field are on the order of -50 dB below the peak amplitudes. For larger measurement radii, the differences are below -60 dB.

The complex differences in the near-field are a good predictor of the far-field differences, so the simulation at representative angles can be used to analyze other AUT/probe/frequency combinations without the need to produce the full near-field and compare the far-fields.

The difference levels are not highly sensitive to the AUT characteristics.   They are slightly lower for the broad beam antenna but the results can probably be applied to a wide range of antenna types.

The primary effect of the higher order probe on the far-field pattern is in the main beam region and the side lobes are relatively unaffected.   This is consistent with the general character of probe correction effects in spherical near-field measurements.

The maximum differences in the peak near-field amplitudes for the two probes was on the order of 0.02 dB and coupled with the observed far-field differences in the main beam region of -53 dB for the 4*MRE radius, any effect on far-field gain should be on the order of hundredths of a dB.

Future work will include extending the study to examine the effects of broadband probes such as open boundary dual ridged probes.

6.0 References

(1) Newell, A.C., Gregson, S.F.," Estimating the effect of higher order modes in spherical near-field probe correction", AMTA 34th Annual Meeting & Symposium, Seattle, WA, Oct. 2012.
(2) Newell, A.C., Gregson, S.F., "Higher Order Mode probes in Spherical Near-Field Measurements", EuCAP, Gothenburg, April, 2013.
(3) Jensen, F. (1975), "On the probe compensation for near-field measurements on a sphere", *Archiv für Elektronik und Übertragung-stechnik*, Vol. 29, No. 7/8, pp. 305-308.
(4) Hansen, J.E. (Ed.) (1988), *Spherical Near-Field Antenna Measurements*, Peter Peregrinus, Ltd., on behalf of IEE, London.
(5) Wacker, P.F. (1974), "Near-field antenna measurements using a spherical scan: Efficient data reduction with probe correction", *Conf. on Precision Electromagnetic Measurements*, IEE Conf. Publ. No. 113, pp. 286-288, London, UK.
(6) Jensen, F., Frandsen, A., "On the number of modes in spherical expansions", AMTA 26th Annual Meeting & Symposium, Stone Mountain, GA, Oct. 2004.
(7) T. A. Laitinen, S. Pivnenko, and O. Breinbjerg, "Odd-order probe correction technique for spherical near-field antenna measurements," *Radio Sci.*, vol. 40, no. 5, 2005.
(8) T. A. Laitinen and O. Breinbjerg, "A first/third-order probe correction technique for spherical near-field antenna measurements using threeprobe orientations," *IEEE Trans. Antennas Propag.*, vol. 56, pp. 1259–1268, May 2008.
(9) T. Laitinen, J. M. Nielsen, S. Pivnenko, and O. Breinbjerg, "On the application range of general high-order probe correction technique in spherical near-field antenna measurements," presented at the 2nd Eur. (EuCAP'07), Edinburgh, U.K., Nov. 2007.
(10) T. A. Laitinen, S. Pivnenko, and O. Breinbjerg," Theory and Practice of the FFT/Matrix Inversion Technique for Probe-Corrected Spherical Near-Field Antenna Measurements With High-Order Probes," *IEEE Trans. Antennas Propag.*, vol. 58,, No. 8, pp. 2623–2631, August 2010.
(11) T. A. Laitinen, S. Pivnenko,"On the truncation of the azimuthal mode spectrum of high-order probes in probe-corrected spherical near-field antenna measurements" AMTA, Denver, November 2012.
(12) Kerns, D.M. (1976), "Plane-wave scattering.matrix theory of antennas and antenna-antenna interactions : formulation and applica-tions", *J. Res. NBS*, Vol. 80B, No. 1, pp. 5-51.